International Journal of Nanomedicine

Dovepress
open access to scientific and medical research

Open Access Full Text Article

ORIGINAL RESEARCH

# Photothermal effects of $NaYF_4$:Yb,Er@$PE_3$@$Fe_3O_4$ superparamagnetic nanoprobes in the treatment of melanoma

This article was published in the following Dove Press journal:
*International Journal of Nanomedicine*

Xue Wang[1]
Chunyang Kang[2]
Ying Pan[1]
Rihua Jiang[3]

[1]Department of Obstetrics & Gynecology, China–Japan Union Hospital of Jilin University, Changchun, People's Republic of China; [2]Department of Neurology, China–Japan Union Hospital of Jilin University, Changchun, People's Republic of China; [3]Department of Dermatology, China–Japan Union Hospital of Jilin University, Changchun, People's Republic of China

**Objective:** The study aimed to synthesize superparamagnetic $NaYF_4$:Yb,Er@$PE_3$@$Fe_3O_4$ upconversion nanoprobes and to study their photothermal effects for the treatment of malignant melanoma.

**Methods:** Morphological characteristics of the synthesized nanoprobes were examined by scanning electron microscopy. Their biocompatibility and biodistribution profiles were assessed through blood routine/biochemistry tests and the inductively coupled plasma/optical emission spectrometry-based analysis of tissue metal elements. Their photothermal conversion efficiency and their potential as contrast agents for upconversion luminescence (UCL)/magnetic resonance imaging (MRI) dual-modal imaging were tested. Efficacy in photothermal therapy, which was achieved by combining nanoprobes with near-infrared (NIR) irradiation, was evaluated in both A375 cell line and BALB/c mice models. The underlying mechanisms were interrogated by molecular approaches including the MTT assay, flow cytometry, semiquantitative PCR, western blot, and immunohistochemistry.

**Results:** 1) Our synthesized $NaYF_4$:Yb,Er@$PE_3$@$Fe_3O_4$ nanoprobes exhibited a uniform cubic morphology with a diameter of ~50 nm. Subcutaneous administration led to no severe, long-lasting adverse effects in mice, possibly due to complete removal of these nanomaterials within one month. 2) Our nanoprobes possessed superior photothermal conversion efficiency and strong contrasting effects during UCL/MRI dual-modal imaging, corroborating their applications in imaging-guided photothermal therapy. 3) Combinatorial treatment of these nanoprobes with NIR irradiation induced profound apoptosis/necrosis in A375 cells. Similarly, the same treatment modality led to strong therapeutic effects in BALB/c mice implanted with A375 tumor xenografts. Mechanistic studies suggested an involvement of heat shock protein 70 in mediating the observed antitumor effects of our nanoprobes.

**Conclusion:** Our study describes a convenient method to synthesize a new type of superparamagnetic upconversion nanoprobes, which possess high biocompatibility and can be used in imaging-guided photothermal therapy for the treatment of malignant melanoma. Importantly, our findings will promote clinical applications of $NaYF_4$:Yb,Er@$PE_3$@$Fe_3O_4$ as novel theranostic agents in treating melanoma and many other tumors.

**Keywords:** upconversion nanoparticles, near infrared, photothermal therapy, melanoma, heat shock protein 70

Correspondence: Rihua Jiang
Department of Dermatology, China–Japan Union Hospital of Jilin University, Changchun, Jilin 130033, People's Republic of China
Tel +861 590 442 8398
Fax +860 431 464 1026
Email jrh1963@163.com

## Introduction

Melanoma represents the most aggressive and the deadliest form of dermatologic cancer. Prognosis of patients with metastatic melanoma is very poor, with only 14% of patients surviving for five years.[1] Current therapeutic options include surgical

resection, chemotherapy, photodynamic therapy, immunotherapy, targeted therapy, and others.[2] However, the efficiency of these treatments commonly decreases due to the development of diverse resistance mechanisms,[3] necessitating a continued search for novel therapeutic strategies with higher efficacy.

In recent years, tremendous advancement in nanotechnology research has provided a variety of multifunctional nanomaterials with unique optical properties, which enables ablation of tumor cells by imaging-guided photothermal therapy (PTT).[4] PPT is minimally invasive and has become a promising cancer treatment modality. It induces local hyperthermia by photothermal coupling agents that convert the highly transmissive near-infrared (NIR) light to heat.[5] Since cancer cells are intolerable of elevated temperature, PTT selectively eradicates them and spares healthy cells intact.[6] Thus, PTT causes few side effects that commonly occur when using conventional therapies. One particular type of such nanomaterials that has provoked widespread interest is lanthanide ($Ln^{3+}$)-doped nanoparticles (eg, $NaYF_4$:Yb,Er) integrated with a superparamagnetic shell (eg, $Fe_3O_4$). Compared to many other hyperthermic agents, $Fe_3O_4$ nanoparticles show a much higher energy conversion efficiency.[7] Markedly, the as-formed $NaYF_4$:Yb,Er@$Fe_3O_4$ nanocore allows for upconversion luminescence (UCL)/magnetic resonance imaging (MRI) dual-modal imaging, which ensures both real-time imaging with high spatial resolution and accurate diagnosis with deep tissue penetration.[8,9]

Although the $Ln^{3+}$-doped magnetic $Fe_3O_4$ nanoparticles usually possess high specific surface area, low toxicity, and good biocompatibility,[10] further surface modifications are usually essential for better clinical applications.[11] Many studies reported the use of polyethylene glycol as an attractive conjugation material.[8,12] However, the presence of polyethylene glycol on the nanoparticle surface reduces cellular uptake, a drawback that can be overcome by replacing with polyelectrolytes (PEs).[13] In fact, PEs have been widely accepted to coat gold nanorods to increase the latter's long-term stability, hydrophilicity, drug delivery capacity, and photothermal activity.[14] The majority of nanoprobes with surface modifications efficiently accumulate at tumor sites due to the enhanced permeability and retention effects of solid tumors.[15] Therefore, modification of the $NaYF_4$:Yb,Er@$Fe_3O_4$ nanocore with PE layers integrates multimodal imaging functions, such as infrared thermal imaging, UCL imaging, and MRI, with effective PTT against cancer cells. However, studies on PE-coated $NaYF_4$:Yb,Er@$Fe_3O_4$ magnetic nanocomposites and their theranostic values are lacking.

We previously reported the synthesis of $NaYF_4$:Yb,Er upconversion nanoparticles (UCNPs) and $Fe_3O_4$ magnetic beads, and characterized their properties, respectively.[10,16] In this study, we fabricated the hybrid $NaYF_4$:Yb,Er@$Fe_3O_4$@$PE_3$ upconversion superparamagnetic nanoprobes, examined their morphology by scanning electron microscopy, and then assessed their biodistributions, biocompatibilities, and capacities as contrasting agents for UCL/MRI dual-modal imaging in BALB/c nude mice. Finally, we evaluated the effectiveness of our nanoprobes as PTT agents both in vitro and in vivo, and proposed putative molecular mechanisms underlying these observed effects (Figure 1).

# Materials and methods

## Chemicals and animals

Benzyl ether, oleic acid, oleylamine, iron (III) acetylacetonate, 3-mercaptopropionic acid, polyethylenimine (molecular weight~25,000), $YCl_3$ (99.99%), $ErCl_3$ (99.99%), poly(allylamine hydrochloride) (PAH; molecular weight≈15,000), and 1-octadecene (90%) were all purchased from Sigma-Aldrich Co. (St Louis, MO, USA). HCl (37%) was supplied by Acros Organics. $NH_4F$ (>98.0%) was obtained from Alfa Aesar. Sodium hydroxide (NaOH), hexane, and chloroform were purchased from Beijing Chemical Works. The BALB/c mice (7–8 weeks old) were provided by the Comparative Medicine Center of Yangzhou University. All animal experiments conducted in the current study were approved by the Institutional Animal Care and Use Committee (IACUC) of Jilin University (including guidelines for animal care, use, and euthanasia).

## Synthesis of $Fe_3O_4$@$PE_3$ nanoparticles

The $Fe_3O_4$ magnetic beads were prepared according to previously reported methods with modifications.[17] Briefly, iron (III) acetylacetonate, 1,2-hexadecanediol, oleic acid, oleylamine, and benzyl ether were mixed under nitrogen flow, and heated up to and remained for 1 h at 200 °C and 300 °C sequentially. After cooling down to room temperature, the resultant $Fe_3O_4$ nanoparticles were precipitated by ethanol, separated by magnetic field, and washed with and finally dispersed in chloroform. To realize biofunctionalization, the as-synthesized $Fe_3O_4$ nanoparticles were coated with polyethylenimine via the ligand exchange approach.[10] Hexane was added to facilitate precipitation of the nanoparticles through vigorous stirring. The as-formed $Fe_3O_4$@$PE_3$ nanoparticles were dispersed in water.

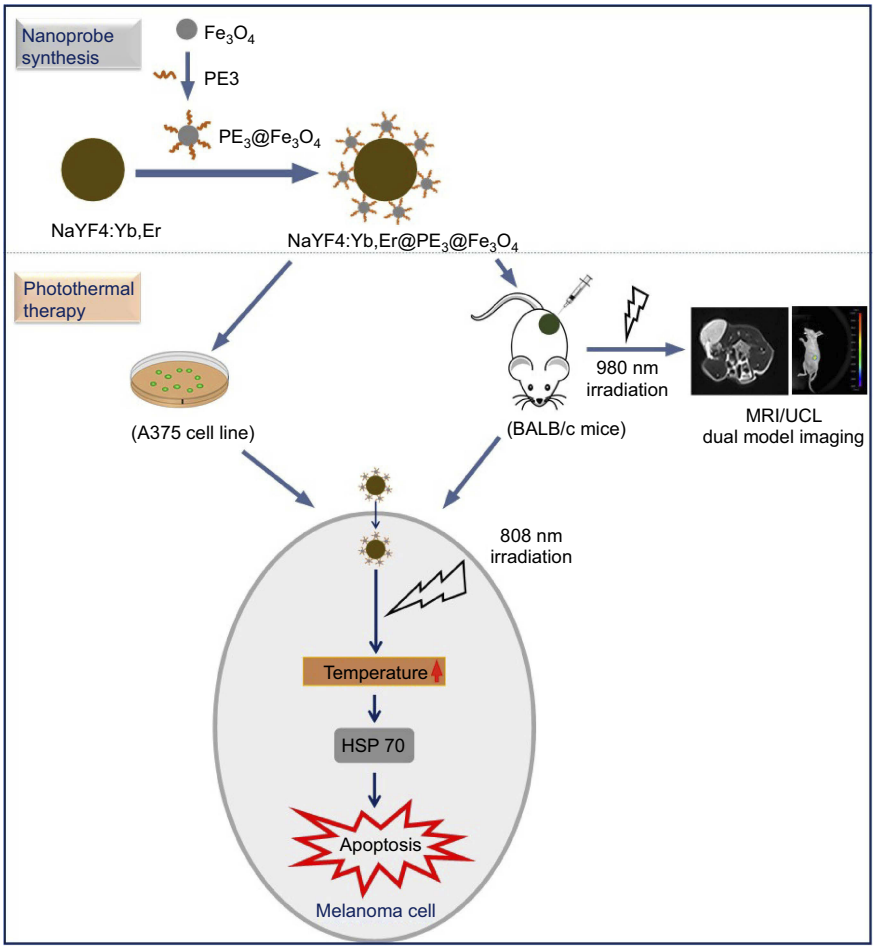


**Figure 1** Schematic diagram for the synthesis of $NaYF_4$:Yb,Er@$PE_3$@$Fe_3O_4$ upconversion nanoprobes and subsequent use in photothermal therapy.
**Abbreviations:** HSP, heat shock protein; MRI, magnetic resonance imaging; UCL, upconversion luminescence.

## Synthesis of $NaYF_4$:Yb,Er upconversion nanoparticles

UCNPs were prepared via high-temperature coprecipitation according to published procedures.[18] Specifically, $YCl_3$, $YbCl_3$, and $ErCl_3$ were mixed with oleic acid and 1-octadecene, stirred for 30 min under a nitrogen atmosphere to remove $O_2$, heated slowly to 160 °C, and maintained for 30 min to dissolve rare earth chlorides completely. After cooling down to room temperature, the solution was added to $NH_4F$ and NaOH dissolved in methanol and heated slowly to 85 °C with stirring until all of the methanol evaporated. Subsequently, the solution was heated to and maintained at 310 °C for 1.5 h under nitrogen protection before cooling down to room temperature. The resultant UCNPs were centrifuged, washed with cyclohexane/ethanol, and redispersed in cyclohexane, followed by surface modification with PAH. To achieve this, hydrophobic oleate-capped UCNPs were first mixed with HCl and stirred for 20 h vigorously to remove oleate ligands from the surface through protonation. Then, UCNPs were incubated with acetone, centrifuged, and washed with water. The water-dissolved UCNPs were then mixed with PAH (0.4 mM in $H_2O$) and stirred for 20 h to complete the reaction. Finally, PAH-capped UCNPs were scrubbed and redispersed in water.

## Synthesis of $NaYF_4$:Yb,Er@$Fe_3O_4$@$PE_3$ nanoprobes

$NaYF_4$:Yb,Er@$Fe_3O_4$@$PE_3$ nanoprobes were prepared following an electrostatic adsorption method. First, $Fe_3O_4$@$PE_3$ was mixed with PAH-capped $NaYF_4$:Yb,Er UCNPs and incubated for 20 min with constant stirring. The final products were retrieved by centrifugation and were dispersed in aqueous solution.

## In vivo biocompatibility and biodistribution

Ten healthy BALB/c mice were injected subcutaneously with 1 mg/mL $NaYF_4$:Yb,Er@$PE_3$@$Fe_3O_4$ nanoprobes (10 mg/kg

body weight) or saline control of equal volume and were maintained in a cage for 1 or 3 months before being sacrificed. The general health status of mice during this period was monitored daily, including body weight, urination, and defecation. Then, fresh blood samples were collected via decapitation and saved into tubes containing EDTA or heparin as anticoagulant for blood routine or biochemical tests, respectively, to evaluate the biocompatibility of the as-synthesized nanoprobes. Meanwhile, various organs (heart, liver, spleen, lung, and kidney) were harvested and subjected to biodistribution analysis of synthesized nanoprobes. Specifically, weighted tissues were mixed with nitric acid and hydrogen peroxide (v:v=1:2), heated to 180 °C at an incremental rate of 10 °C per minute, and incubated for 40 min for nitrification. After cooling down, the as-obtained extracts were deprived of acid and subsequently measured by inductively coupled plasma optical emission spectrometry to determine the biodistribution of $NaYF_4$:Yb,Er@$PE_3$@$Fe_3O_4$ nanoprobes.

## In vivo thermal imaging and upconversion fluorescence imaging

BALB/c mice were anesthetized using trichloroacetaldehyde hydrate (10%) at a dosage of 40 mg/kg and injected subcutaneously in the exterior aspect of the left hind leg with either 0.2 mg $NaYF_4$:Yb,Er@$PE_3$@$Fe_3O_4$ nanoprobes or saline control of equal volume. Then, mice were irradiated for 5 min by 808-nm laser within an area 2 mm in diameter at a power of 0.5 W. During the laser irradiation, infrared thermal images were captured using an IR camera of a PTT monitoring system (Fotric 225–3). For upconversion fluorescence imaging, anesthetized mice were injected subcutaneously with 0.2 mg $NaYF_4$:Yb,Er@$PE_3$@$Fe_3O_4$ nanoprobes in the left flank. Then, they were irradiated with a 980-nm NIR laser at power of 0.5 W in a small animal fluorescence imaging system (NightOWL LB 983; Berthold). The emission light from $NaYF_4$:Yb,Er@$PE_3$@$Fe_3O_4$ nanoprobes was collected at 550 nm.

## Cell culture

The A375 melanoma cell line was provided by the Core Laboratory at China–Japan Union Hospital of Jilin University. Use of this cell line was approved by the Animal Experimental Ethical Inspection Committee at Jilin University (Permit no.: 201802034). Cells were cultured in RPMI 1640 medium supplemented with 10% FBS and 1% penicillin/streptomycin. Cells were maintained within a 37 °C incubator under exposure to 5% $CO_2$. When reaching 70–80% confluence, cells were treated for 24 h with 1 mg/mL $NaYF_4$:Yb,Er@$PE_3$@$Fe_3O_4$ nanoprobes, followed by Prussian staining and confocal fluorescence imaging (FV1000; Olympus Corporation, Tokyo, Japan) to examine cellular uptake of the nanoprobes.

## In vitro cytotoxicity assay

In vitro cytotoxicity was evaluated using the MTT assay according to the vendor's instructions. Briefly, A375 cells were seeded in a 96-well plate at a density of 1,000 cells per well and equilibrated for 24 h at 37 °C before they were treated either with nanoprobes at increasing concentrations of 0.125, 0.25, 0.5, and 1 mg/mL or with vehicle control. Then, all of the cells were either left undisturbed or irradiated with an 808-nm NIR laser for 10 min using a power of 1 W. Twenty-four hours later, cells were imaged by light microscope and subjected to MTT assay, wherein optical absorbance was measured at 490 nm using a microplate reader. Cell viability was calculated as a percentage of the control group. All experiments were repeated three times.

## Flow cytometry

When reaching 80% confluence, A375 cells were seeded in a 6-well plate at a density of $2\times10^6$ cells/mL and equilibrated for 24 h, before they were treated either with 1 mg/mL nanoprobes or with vehicle control for 4 h. Then, all cells followed the same irradiation protocol as mentioned above. After another 24 h, cells were harvested by trypsinization, washed twice with PBS, and pelleted by centrifugation at 2,000 rpm for 5 min. A total of $1\times10^6$ cells were then resuspended in Annexin V binding buffer containing 5 μL of 0.5 mg/mL propidium iodide and 5 μL of Annexin V–fluorescein isothiocyanate, and incubated for 15 min at room temperature in the dark. Samples were analyzed in a FACSCalibur flow cytometer (BD Biosciences, San Jose, CA, USA). The 488-nm laser was selected for excitation. The 520 nm and 620 nm channels were used for emission of fluorescein isothiocyanate and propidium iodide, respectively. At least 10,000 events of single cells per sample were collected. All experiments were repeated three times.

## Western blot

A375 cells growing in a 6-well plate were either left intact (as control) or treated for 4 h with $NaYF_4$:Yb,Er@$PE_3$@$Fe_3O_4$ nanoprobes at concentrations of 0.25 mg/mL or 1 mg/mL.

Then, nanoprobe-treated cells were irradiated with an 808-nm NIR laser for 10 min at a power of 1 W. After 24 h, whole cellular protein lysates were prepared by in-well scrapping in RIPA buffer supplemented with protease inhibitors (Hoffmann-La Roche Ltd., Basel, Switzerland), followed by centrifugation at 12,000×g for 10 min at 4 °C to save the supernatant. Protein concentrations were determined by the BCA Protein Assay Kit according to the manufacturer's instructions (Thermo Fisher Scientific, Waltham, MA, USA). Western blot was performed as previously described with modifications.[19] Briefly, proteins were resolved by SDS-PAGE, transferred to nitrocellulose membranes, and blocked with 5% nonfat milk for 1 h at room temperature. After overnight incubation with anti-HSP70 primary antibody at 4 °C (Cell Signaling Technologies), membranes were washed with TBST three times and incubated for 1 h at room temperature with horseradish peroxidase-conjugated goat anti-rabbit secondary antibody (Thermo Fisher Scientific). Membranes were washed three times with TBST and rinsed in $H_2O_2$/DAB substrate mixture until reaction proceeding to the desired intensity (Thermo Fisher Scientific). Finally, membranes were washed in water, dried, and photographed. Densitometric quantification analysis was performed using ImageJ software.

## Semiquantitative reverse transcription-PCR (RT-PCR)

Total RNAs were isolated from A375 cells via the TRIzol method following the vendor's manual (Invitrogen; Thermo Fisher Scientific) and quantified by NanoDrop. After DNase I treatment (Hoffmann-La Roche), 1 µg RNA was reverse-transcribed to cDNA using the HiScript II 1st Strand cDNA Synthesis Kit (Vazyme). Benchtop PCR was performed on a GeneAmp PCR System 9700 machine in a 50 µl reaction volume: 1× PCR buffer (+$Mg^{2+}$), 0.2 mM dNTP, 0.2 µM primers, 50 ng of template cDNA, and 0.5 µL of Platinum TaqDNA polymerase (Invitrogen). The cycling parameters used were as follows: initial 94 °C for 5 min, followed by 30 cycles of 94 °C for 30 s, 55 °C for 30 s, and 72 °C for 60 s; an additional extension at 72 °C for 7 min; and finally held at 4 °C. The PCR products were resolved by electrophoresis using agarose gels supplemented with ethidium bromide. Images of bands were acquired by the ChemiDoc™ MP Imaging System (Bio-Rad Laboratories Inc., Hercules, CA, USA) and quantification was performed using the built-in Image Lab software. Relative expression levels were presented as ratios of band intensities of heat shock protein HSP70 over the internal control gene GAPDH. Sequences of all primers are shown in Table 1.

## In vivo photothermal therapy

BALB/c nude mice (average body weight 20 g) were injected subcutaneously in the dorsal side of the right hind leg with $2\times10^6$ A375 cells resuspended in saline and reared for 4 days when tumors grew to at least 5 mm in diameter. Then, tumor-bearing mice were anesthetized and injected intratumorally with 100 µL of either 1 mg/mL nanoprobes or saline. Immediately, these mice were irradiated with an 808-nm NIR laser for 5 min or left undisturbed. This irradiation procedure was repeated every 12 h for a total of four times, finally generating the following treatment groups: 1) saline alone; 2) saline+NIR; 3) nanoprobes alone; and 4) nanoprobes+NIR. Naïve tumor-free BALB/c nude mice served as normal control. Body weight, tumor volume, and abnormal behaviors were recorded every 2 days for the duration of the study.

## Magnetic resonance imaging

Five days post PTT, mice were anesthetized with trichloroacetaldehyde hydrate. Sequential MRI acquisitions were performed on a 7 T Siemens Magnetom Trio system. T1- and T2-weighted MRI maging was done with the following parameters: TR/TE=1500/32 ms, matrix size=256×256, field of view=30 mm×30 mm, slice thickness=1.5 mm, scan time~10 min.

## Histological analysis

At the end of in vivo PTT, mice were euthanized and fixed with 4% paraformaldehyde via intracardiac perfusion.

**Table 1** PCR primers

| Gene name | Primer sequence | | $T_m$ (°C) |
|---|---|---|---|
| HSP70 | Forward<br>Reverse | TTTTGGTCCTAAGAATCGTTCA<br>ACACTTTCGGCTGTCTCCTTCA | 54.5<br>60.1 |
| GAPDH | Forward<br>Reverse | GGGTGATGCTGGTGCTGAGTATGT<br>AAGAATGGGTGTTGCTGTTGAAGTC | 57.0<br>57.0 |

Major organs (heart, liver, spleen, lung, and kidney) were harvested and sliced for H&E staining to assess the morphological integrity. Tumor tissues were also collected, sectioned, and analyzed by immunohistochemistry to investigate the expression of HSP70 according to a standard protocol.[20] Images were captured using a bright-light microscope (Olympus).

### Statistical analyses

All of our data were analyzed using GraphPad Prism, then expressed as mean±SD. One-way ANOVA was applied for comparison among multiple groups, followed by post hoc test. Student's t test (two-tailed) was used for difference comparison between two groups. All statistical differences with $p<0.05$ were considered significant.

## Results and discussion

### Characterization of $NaYF_4$:Yb,Er@$PE_3$@$Fe_3O_4$ nanoprobes

Scanning electron microscopy examination of the as-synthesized $NaYF_4$:Yb,Er@$PE_3$@$Fe_3O_4$ nanoprobes showed a uniform cube morphology with a mean diameter of ~50 nm, larger than our previously reported UCNPs,[16] confirming successful encapsulation with $Fe_3O_4$ and $PE_3$ layers (Figure 2A). Their superparamagnetic properties were demonstrated by guided movement to the target position in the presence of an external magnetic field (Figure 2B), suggesting their potential role in enhanced MRI. The luminescence spectrum of the nanoprobes dispersion exhibited three characteristic emission peaks located at 525 nm, 545 nm, and 660 nm under excitation at 980 nm (Figure 2C), validating their usage as contrast agents during UCL imaging. Altogether, our data confirmed successful fabrication of the superparamagnetic $NaYF_4$:Yb,Er@$PE_3$@$Fe_3O_4$ upconversion nanoprobes with a uniform size and morphology, indicating their potentials for UCL/MRI dual-modal imaging-guided PTT.

### In vivo biocompatibility and biodistribution

To test the biocompatibility of the as-synthesized $NaYF_4$:Yb,Er@$PE_3$@$Fe_3O_4$ nanoprobes, we injected healthy BALB/c mice subcutaneously with either saline or nanoprobes (1 mg/mL), and monitored their general health status. One month and three months later, blood samples were collected and subjected to blood routine/biochemical tests. None of the blood routine tests showed abnormalities between nanoprobe- and saline-injected mice, except for the number of platelets that first decreased at month one and then recovered to normal levels by month three (Table 2). Similarly, no abnormalities were observed in blood biochemical tests, except for alanine aminotransferase that increased at month one but returned to normal levels by month three (Table 3). However, two other indices for liver function, aspartate aminotransferase and alkaline phosphatase, remained unchanged. Although these data indicated slight disturbance to the liver, all experimental mice showed no signs of anxiety, distress, or pain. In summary, our data suggested low in vivo toxicity of as-synthesized nanoprobes.

To determine the biodistribution and clearance dynamics of our nanoprobes in vivo, blood as well as major organs (heart, liver, spleen, lung, kidney) were harvested from nanoprobe-injected mice, one month after injection, and processed for inductively coupled plasma optical emission spectrometry analysis to measure the tissue contents of Fe, Yb, and Er (Table 4). Saline-injected mice served as controls. Our results showed that Fe was detectable in all of the harvested tissues and the contents exhibited no differences between the two groups, except in the tissue of the liver where its concentrations were higher in the nanoprobe group. These findings, together with blood alanine aminotransferase test results, suggested clearance of our nanoprobes through the hepatic route. In contrast, Yb was only present in the kidney with similar tissue contents between the two groups. Er was detected in the blood and kidney of both groups, and its tissue contents remained unaltered. However, administration of nanoprobes indeed led to additional accumulation of Er in the spleen and lung. These results are in accordance with the spleen as the largest immune organ, since a strong interaction has been demonstrated between nanoparticles and the immune system.[21] Altogether, our findings showed that majority of injected $NaYF_4$:Yb,Er@$PE_3$@$Fe_3O_4$ nanoprobes were secreted out within a month, suggesting negligible long-term systemic retention.

### In vivo photothermal effects

To test the photothermal conversion efficiency of $NaYF_4$:Yb,Er@$PE_3$@$Fe_3O_4$ nanoprobes, BALB/c nude mice were injected subcutaneously with nanoprobes (10 mg/kg body weight) in the exterior aspect of the left hind leg. Mice injected with saline served as controls. Both groups were irradiated at the injection site with an 808-nm NIR laser for 5 min. Full-body

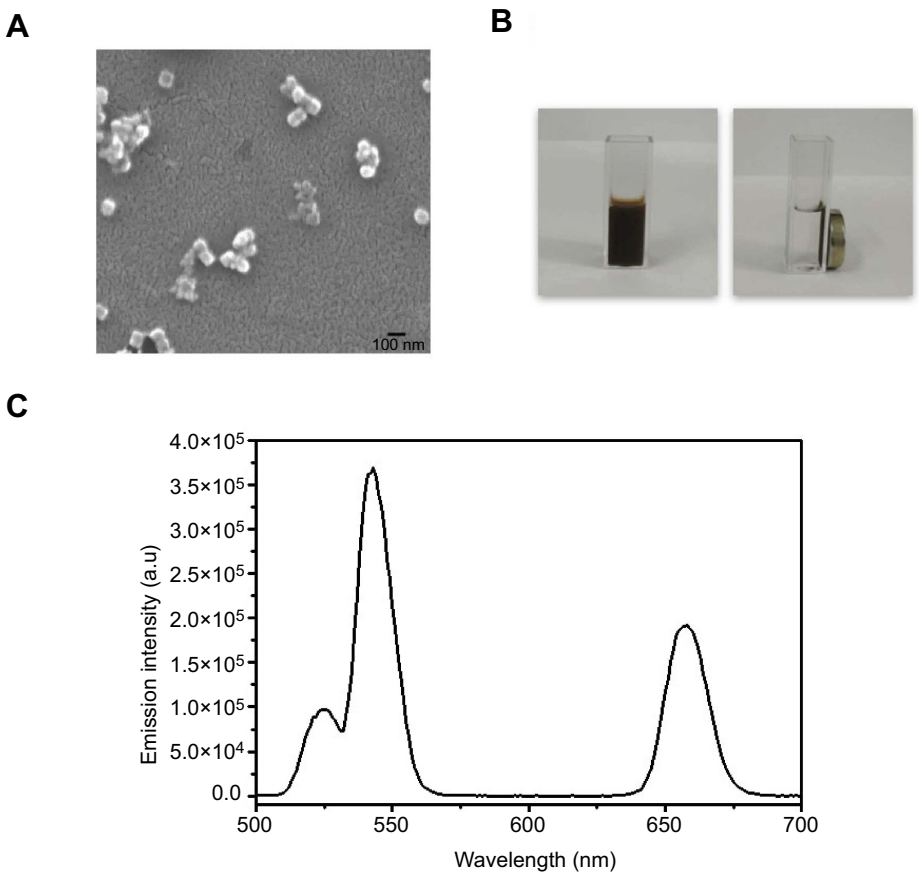


**Figure 2** Characterization of the superparamagnetic $NaYF_4$:Yb,Er@$PE_3$@$Fe_3O_4$ upconversion nanoprobes. (**A**) Scanning electron microscopy image revealing cubic morphology of these nanoprobes with a uniform diameter of ~50 μm. Scale bar, 100 μm. **(B)** Images of synthesized nanoprobes dispersed in an aqueous solution in the absence (left) and presence (right) of a neighboring magnet. (**C**) Upconversion emission spectra of synthesized nanoprobes under 980 nm laser excitation, with a major peak centered at 550 nm.

**Table 2** Blood routine tests after in vivo administration of synthesized nanoprobes

| | Baseline | Month one | Month three |
|---|---|---|---|
| WBC ($10^9$/L) | 6.7±1.7 | 5.5±1.2 | 6.5±1.4 |
| HGB (g/dL) | 14.3±1.9 | 15.4±2.3 | 14.9±2.1 |
| PLT ($10^9$/L) | 49±18 | 39±15 | 42±16 |
| GRANS ($10^9$/L) | 2.5±1.1 | 2.8±1.4 | 2.6±1.3 |
| % GRANS | 37±11 | 50±16 | 43±13 |
| HCT (%) | 53.8±1.3 | 55.6±1.8 | 55.1±1.4 |
| MCHC (g/dL) | 28.9±1.7 | 25.8±2.6 | 26.8±2.1 |
| L/M ($10^9$/L) | 4.2±2.1 | 1. 3.9±1.5 | 3.9±1.8 |
| % L/M | 63±9 | 44±11 | 49±9 |
| RETICS (%) | 0.7±0.3 | 0.5±0.2 | 0.6±0.3 |

**Note:** Data were expressed as mean±SD, n=6.
**Abbreviations:** WBC, white blood cells; HGB, hemoglobin; PLT, platelets; GRANS, granulocytes; HCT, hematocrit; MCHC, mean corpuscular hemoglobin concentration; L/M, lymphocytes; RETICS, reticulocytes.

infrared thermal images and changes of local temperature were recorded (Figure 3A and B). Our results showed that as irradiation prolonged, the temperature steadily rose in nanoprobe-injected mice, reaching 33.8, 42.2, 50.9, 55.2, 60.1, and 62.0 °C after irradiation for 0.5, 1, 2, 3, 4, and 5 min, respectively. These increments quickly relapsed after cessation of irradiation, whereby the local temperature dropped almost to the baseline level of 25.6 °C within 5 min. In contrast, temperature increments in saline-injected control mice under the same conditions were much smaller. Thus, these findings validated our synthesized nanoprobes as photothermal agents with strong light-to-heat conversion efficiency.

## In vivo UCL imaging

To test the potential of our nanoprobes as contrast agents for UCL imaging, we injected BALB/c mice with nanoprobes and placed them within a small animal fluorescence imaging system. In vivo UCL imaging was accomplished by inverted fluorescence microscopy under the excitation of a 980-nm NIR laser. As presented in Figure 3C, nanoprobe-bearing

**Table 3** Blood biochemical tests after in vivo administration of synthesized nanoprobes

| | Baseline | Month one | Month three |
|---|---|---|---|
| ALT (U/L) | 60±25 | 126±53* | 66±28 |
| AST (U/L) | 23±19 | 39±21 | 28±17 |
| ALP (U/L) | 135±46 | 142±41 | 138±38 |
| AMYL (U/L) | >2,500 | >2,500 | >2,500 |
| LAC (mmol/L) | 7.01±2.31 | 6.31±2.52 | 6.58±1.93 |
| Urea (mmol/L) | 5.2±1.3 | 5.9±1.7 | 5.5±1.4 |
| CREA (μmol/L) | 25±9 | 15±11 | 17±10 |
| GLU (mmol/L) | 9.23±1.06 | 8.9±1.53 | 9.11±1.13 |
| TBIL (μmol/L) | 8±5 | 10±5 | 8±4 |
| TP (g/L) | 65±11 | 68±14 | 65±12 |
| ALB (g/L) | 29±6 | 24±8 | 26±7 |
| CHOL (mmol/L) | 2.93±0.91 | 2.59±1.37 | 2.66±1.14 |

**Note:** Data were expressed as mean±SD, n=6. *$p<0.05$.
**Abbreviations:** ALT, alanine aminotransferase; AST, aspartate aminotransferase; ALP, alkaline phosphatase; AMYL, amylase; LAC, lactate; CREA, creatinine; GLU, glucose; TBIL, total bilirubin; TP, total protein; ALB, albumin; CHOL, cholesterol.

mice manifested a strong UCL signal only at the injection site, with almost no autofluorescence elsewhere. Our observations verified the feasibility of $NaYF_4$:Yb,Er@$PE_3$@$Fe_3O_4$ as a sensitive probe for UCL imaging-guided PTT in vivo.

## In vitro photothermal therapy

To evaluate the cellular uptake capacity of our nanoprobes in vitro, we first incubated A375 cells with 1 mg/mL nanoprobes for 12 h and stained with Prussian blue. Using confocal fluorescence microscopy, we detected strong green signals in the cytoplasmic and nuclear fractions, suggesting that our synthesized nanomaterials were readily taken up by A375 cells (Figure 4A). Interestingly, 24-h incubation with 1 mg/mL nanoprobes and subsequent NIR irradiation led to overt cellular apoptosis and necrosis, which were represented by morphological abnormalities, membrane segmentation, and nuclei pyknosis (Figure 4B). In contrast, A375

**Table 4** Biodistribution of metal elements in organs of mice by inductively coupled plasma optical emission spectrometry analysis

| | Blood | | Heart | | Liver | | Spleen | | Lung | | Kidney | |
|---|---|---|---|---|---|---|---|---|---|---|---|---|
| | C | T | C | T | C | T | C | T | C | T | C | T |
| Fe | 46±15.1 | 60±22.9 | 22±10.6 | 8±4.5 | 2.8±0.3 | 61±5.2* | 23±9.1 | 18±3.6 | 16±3.3 | 38±8.5 | 51±24.2 | 12±5.5 |
| Yb | | | | | | | | | | | 1.5±0.8 | 1.3±0.2 |
| Er | 130±41.1 | 166±65.8 | | | | | | 42±17.4 | | 71±12 | 27±10.7 | 41±19.6 |

**Note:** Expressed as fractions of tissue weight, mean±SD×$10^{-5}$ (n=6). *$p<0.05$, C compared to T.
**Abbreviations:** C, saline control; T, nanoprobes treated; Fe, ferric iron; Yb, ytterbium; Er, erbium.

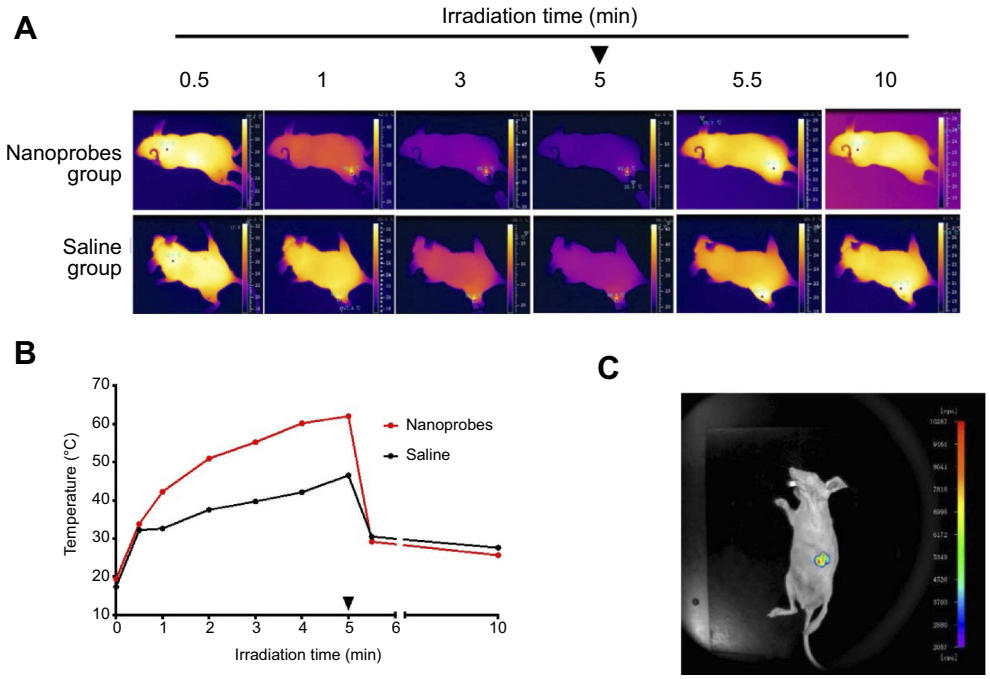


**Figure 3** Near-infrared (NIR) photothermal effects and upconversion luminescence (UCL) imaging in BALB/c mice. (**A**) Thermal imaging of BALB/c mice during NIR irradiation after intratumoral injection of $NaYF_4$:Yb,Er@$PE_3$@$Fe_3O_4$ nanoprobes. The black arrowhead indicates when irradiation ceased. (**B**) Changes of temperature at tumor site during NIR irradiation. The arrowhead indicates when NIR irradiation ceased. **(C)** In vivo UCL imaging after intratumoral injection of nanoprobes.

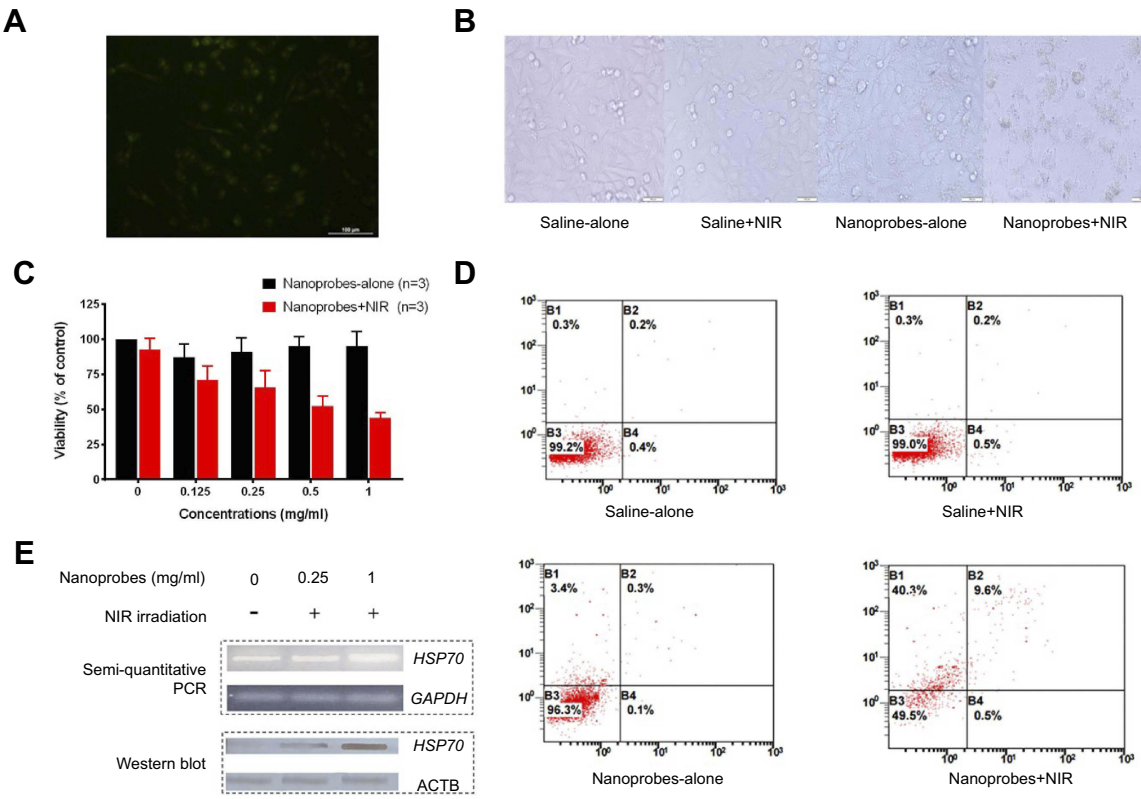


**Figure 4** In vitro photothermal effects in A375 cells. (**A**) Confocal microscope image of cells treated with $NaYF_4$:Yb,Er@$PE_3$@$Fe_3O_4$ nanoprobes and stained with Prussian blue, indicating our nanoprobes were readily taken up by A375 cells. (**B**) Bright-field images of A375 cells treated with saline or nanoprobes, in the presence or absence of near-infrared (NIR) irradiation. The combination of nanoprobes with NIR irradiation led to overt cell death. This experiment was repeated three times. **(C)** MTT assay showing the viability of A375 cells treated with increasing concentrations of nanoprobes in the presence and absence of NIR irradiation (n=3). **(D)** Apoptotic and necrotic rates of A375 cells after photothermal treatment as revealed by flow cytometry. This experiment was repeated three times. **(E)** Expression of heat shock protein HSP70 was elevated with increasing concentrations of nanoprobes in the presence of NIR irradiation, on both mRNA and protein levels as revealed by semiquantitative PCR and western blot, respectively. This experiment was repeated three times.

cells from the nanoprobe-alone and irradiation-alone groups seemed as healthy as the saline-alone control group. To further confirm their photothermal effects, nanoprobes at increasing concentrations (0.125, 0.25, 0.5, and 1 mg/mL) were used to treat A375 cells, which were then subjected to 808-nm irradiation for 10 min or left undisturbed. The MTT assay showed that neither the irradiation-alone nor nanoprobe-alone groups had adverse effects on cell viabilities. However, a combination of nanoprobes with irradiation led to significantly decreased cell viabilities in a dosage-dependent manner. Particularly, the strongest effect was observed for 1 mg/mL nanoprobes, which reduced cell viability to 44% (Figure 4C). These findings were supported by flow cytometric analysis, which utilized Annexin V and propidium iodide to quantitate apoptosis and necrosis, respectively. We found that the percentage of apoptotic/necrotic cells increased dramatically from 0.9% in the saline-alone control group to 50.5% in the the nanoprobes+NIR group (Figure 4D). Again, the nanoprobe-alone and irradiation-alone groups exhibited no differences in apoptosis or necrosis percentages compared to the control group. In sum, our results demonstrated a high efficiency of nanoprobe uptake into A375 cells and confirmed a strong photothermal potential for tumor ablation.

HSP70 is frequently activated in response to heat stress and represents the major molecular chaperone system that assists protein-folding.[22] To gain further insights into mechanisms underlying our nanoprobe-mediated PTT, we treated A375 cells for 24 h with nanoprobes at concentrations of 0.25 and 1 mg/mL, followed by 808-nm laser irradiation. Undisturbed naïve cells served as normal controls. Then, we measured HSP70 expression by semiquantitative RT-PCR and western blot. To our expectations, we observed a significant upregulation of HSP70, on both mRNA and protein levels, with increased concentrations of nanoprobes, implying a critical role of HSP70 in mediating the observed photothermal effects (Figure 4E).

## In vivo photothermal therapy

To test the photothermal effects of $NaYF_4$:Yb,Er@$PE_3$ @$Fe_3O_4$ in vivo, we intratumorally injected BALB/c nude mice bearing A375 tumor xenografts with either 1 mg/mL nanoprobes or saline. Then, mice were left undisturbed or irradiated repeatedly with an 808-nm NIR laser for 5 min per time and four times in total, generating the following treatment groups: 1) saline alone; 2) saline +NIR; 3) nanoprobes alone; and 4) nanoprobes+NIR. Body weights and tumor volumes were inspected and recorded every other day over 10 days (Figure 5A). As expected, body weights of tumor-free mice kept increasing during the entire study (data not shown). In contrast, body weights of tumor-bearing mice in the saline-alone group first increased until day 4 and then started decreasing afterward until day 10, a pattern of changes comparable

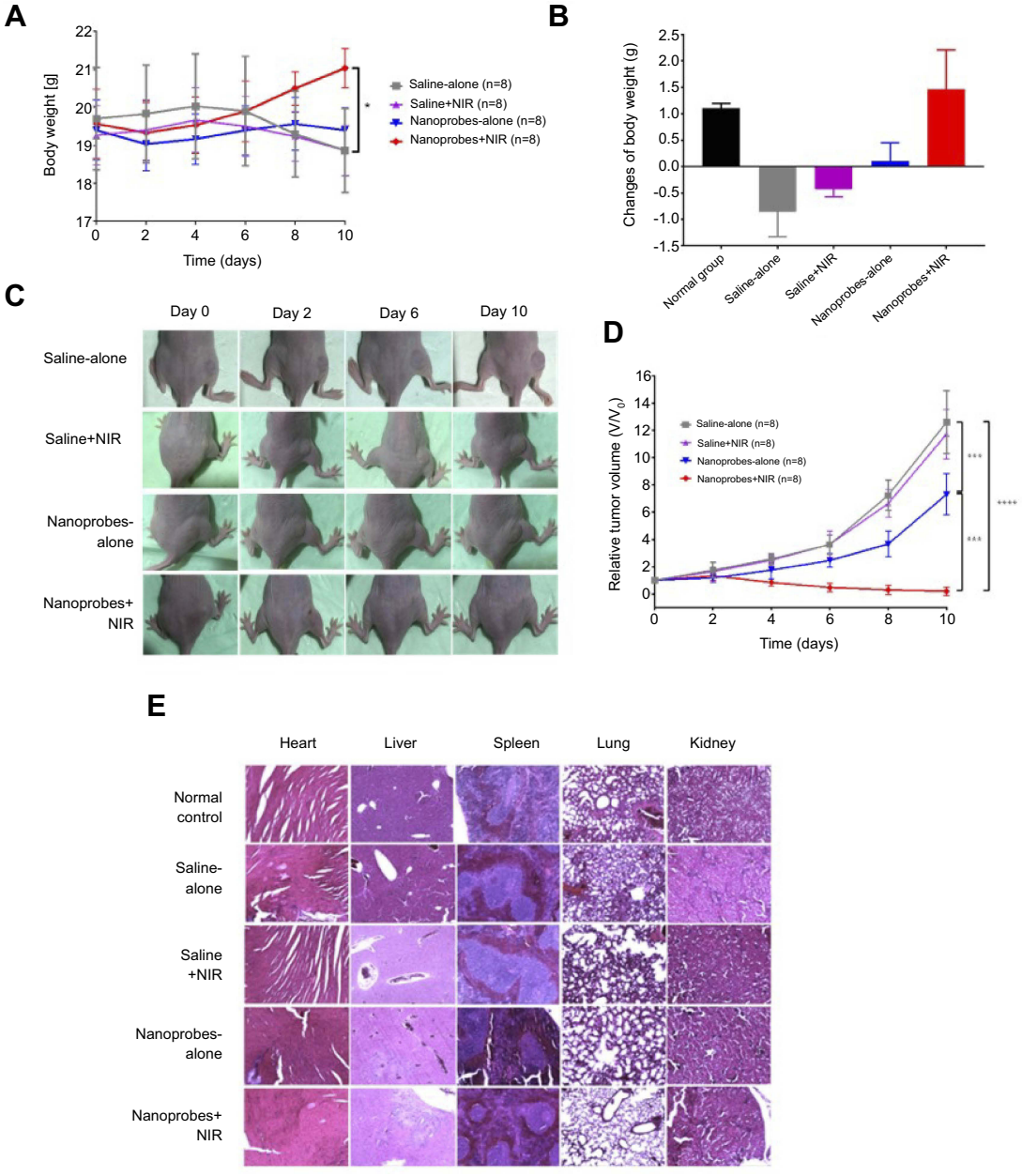


**Figure 5** In vivo photothermal effects in tumor-bearing BALB/c mice. (**A**) Changes of mice body weights over the study (n=8). (**B**) Net changes in body weight by the end of the study in each group (day 10 versus day 0) (n=8). (**C**) Representative photographs of tumors in each treatment group over the study. (**D**) Tumor growth curves of each treatment group (n=8). Tumor sizes were normalized to their initial sizes (baseline) and expressed as fold-change over the latter. (**E**) H&E staining of major organs (heart, liver, spleen, lung, and kidney) in each treatment group. Naïve BALB/c mice were included as normal control. This experiment was repeated three times. *$p$<0.05, ***$p$<0.001, ****$p$<0.0001.

**Abbreviation:** NIR, near infrared.

to that observed in the saline+NIR group, suggesting that NIR irradiation per se exerted no adverse effects on mice. On the contrary, body weights of both the nanoprobe-alone and nanoprobes+NIR groups first dropped in the first 2 days, but quickly recovered over the rest days. Notably, net changes of body weight at day 10 versus day 0 were +1.3, −0.5, −0.3, −0.3, and +0.9 g for the normal, saline-alone, saline+NIR, nanoprobes-alone, and nanoprobes +NIR groups, respectively, validating the ameliorating effects of PTT on mice health conditions (Figure 5B).

In the saline-alone group, the tumor volume increased by 12.6-fold at day 10 compared to that at day 0 (Figure 5C and D). A similar rate of tumor growth was observed for the saline+NIR group, confirming the amenable effects of NIR light to biological tissues. Interestingly, tumor growth in the nanoprobe-alone group was deferred compared to the saline-alone control, possibly attributed to systemic antitumor immune responses stimulated by exogenous nanoparticles.[21] To our expectations, a combination of nanoprobes with NIR irradiation caused tumors to recede dramatically, with an inhibition efficiency being 96.8% at day 10. Besides, no abnormalities in general health status, defecation, or urination were seen for all mice (data not shown). In keeping, morphological examination of major organs by H&E staining showed no signs of damage or structural abnormalities in any treatment groups (Figure 5E), findings that were consistent with earlier biocompatibility study. Altogether, our results verified the therapeutic efficacy of $NaYF_4$:Yb,Er@$PE_3$@$Fe_3O_4$ nanoprobes as strong photothermal coupling agents to eradicate tumors in vivo.

## Tumor size measured by MRI

To evaluate the use of $NaYF_4$:Yb,Er@$PE_3$@$Fe_3O_4$ nanoprobes as contrast agents for MRI to assess therapeutic outcomes of PTT, we performed MRI with tumor-bearing mice that had received PTT for 5 days, at which time both T1- and T2-weighted images were captured (Figure 6A). To our expectations, we observed strong magnetic resonance signals at the tumor sites, confirming the capacity of our nanoprobes to enhance magnetic resonance contrast during MRI. Although nanoprobes alone showed somewhat therapeutic effects, additional NIR irradiation significantly improved this effect and eliminated tumor xenografts to a large extent by the end of PTT. NIR irradiation alone failed to show any effects. To further explore mechanisms underlying photothermal effects, we performed immunohistochemistry to check the expression of tumoral HSP70 in the control (saline-alone) and PTT (nanoprobes+NIR) groups. In line with our in vitro results, we found HSP70 to be dramatically upregulated by PPT (Figure 6B), confirming the involvement of HSP70 in mediating PTT effects of $NaYF_4$:Yb,Er@$PE_3$@$Fe_3O_4$ nanoprobes.

## Conclusion

In this study, we developed a functional $NaYF_4$:Yb,Er@$PE_3$@$Fe_3O_4$ upconversion superparamagnetic nanoprobe for UCL/MRI dual-modal imaging-guided PTT against melanoma, using the A375 cell line and xenografted BALB/c mice as models. First, scanning electron microscopy analysis of our nanoprobes revealed a uniform cube morphology with a diameter of ~50 nm. In vivo biocompatibility studies showed no major systemic toxicity, and biodistribution results suggested the hepatic route as a major clearance pathway. Second, the as-synthesized nanoprobes achieved strong UCL/MRI dual-modal imaging in vivo, laying down an experimental basis for their future applications in simultaneous diagnostics, therapeutics, and prognosis of tumors. In keeping with their superior photothermal conversion efficiency, NIR-irradiated nanoprobes induced overt

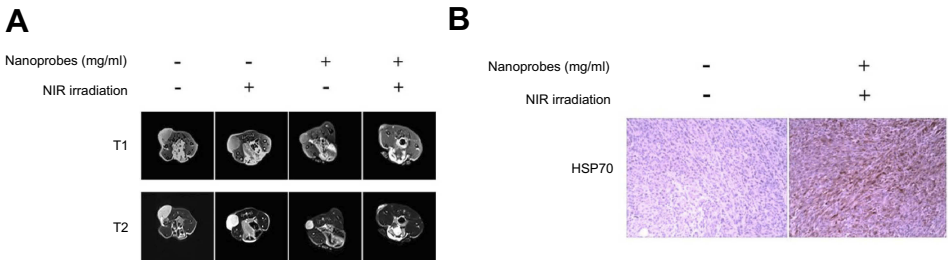


**Figure 6** In vivo magnetic resonance imaging (MRI) scans and tumoral heat shock protein HSP70 expression. (**A**) Tumor-bearing BALB/c mice were intratumorally injected with saline or $NaYF_4$:Yb,Er@$PE_3$@$Fe_3O_4$ nanoprobes, followed by either near-infrared irradiation (NIR) irradiation or not. Five days later, both T1- and T2-weighted MRI scans were captured from each treatment group. (**B**) Immunohistochemical analysis of tumoral HSP70 expression in control mice and those receiving photothermal therapy. This experiment was repeated three times.

apoptosis in A375 melanoma cells, as revealed by in vitro cytotoxicity assay. Of particular note is the strong antitumor efficacy of NIR-irradiated nanoprobes in vivo, which nearly eradicated implanted tumor xenografts in BALB/c mice. Last, we discovered HSP70 as a plausible mechanism underlying the observed antitumor effects. Altogether, findings of current study will promote clinical applications of $NaYF_4$:Yb,Er@$PE_3$@$Fe_3O_4$ nanoprobes as novel theranostic agents in the treatment of melanoma.

## Acknowledgment

The project was supported by the Natural Science Foundation of Jilin Province (Grant No. 20190201205JC).

## Author contributions

All authors contributed to data analysis, drafting or revising the article, gave final approval of the version to be published, and agree to be accountable for all aspects of the work.

## Disclosure

The authors report no conflicts of interest in this work.

## References

1. Miller AJ, Mihm MC Jr. Melanoma. *N Engl J Med*. 2006;355(1):51–65. doi:10.1056/NEJMra052166
2. Leonardi GC, Falzone L, Salemi R, et al. Cutaneous melanoma: from pathogenesis to therapy (Review). *Int J Oncol*. 2018;52(4):1071–1080.
3. Domingues B, Lopes JM, Soares P, Populo H. Melanoma treatment in review. *Immunotargets Ther*. 2018;7:35–49. doi:10.2147/ITT.S134842
4. Hirsch LR, Stafford RJ, Bankson JA, et al. Nanoshell-mediated near-infrared thermal therapy of tumors under magnetic resonance guidance. *Proc Natl Acad Sci U S A*. 2003;100(23):13549–13554. doi:10.1073/pnas.2232479100
5. O'Neal DP, Hirsch LR, Halas NJ, Payne JD, West JL. Photo-thermal tumor ablation in mice using near infrared-absorbing nanoparticles. *Cancer Lett*. 2004;209(2):171–176. doi:10.1016/j.canlet.2004.02.004
6. Huang X, Jain PK, El-Sayed IH, El-Sayed MA. Plasmonic photothermal therapy (PPTT) using gold nanoparticles. *Lasers Med Sci*. 2008;23(3):217–228. doi:10.1007/s10103-007-0470-x
7. Chu M, Shao Y, Peng J, et al. Near-infrared laser light mediated cancer therapy by photothermal effect of $Fe_3O_4$ magnetic nanoparticles. *Biomaterials*. 2013;34(16):4078–4088. doi:10.1016/j.biomaterials.2013.01.086
8. Liu B, Li C, Ma P, et al. Multifunctional $NaYF_4$:Yb, Er@$mSiO_2$@$Fe_3O_4$-PEG nanoparticles for UCL/MR bioimaging and magnetically targeted drug delivery. *Nanoscale*. 2015;7(5):1839–1848. doi:10.1039/C4NR05342G
9. Mi C, Zhang J, Gao H, et al. Multifunctional nanocomposites of superparamagnetic ($Fe_3O_4$) and NIR-responsive rare earth-doped up-conversion fluorescent ($NaYF_4$: Yb,Er) nanoparticles and their applications in biolabeling and fluorescent imaging of cancer cells. *Nanoscale*. 2010;2(7):1141–1148. doi:10.1039/c0nr00102c
10. Ding Y, Cong T, Chu X, Jia Y, Hong X, Liu Y. Magnetic-bead-based sub-femtomolar immunoassay using resonant Raman scattering signals of ZnS nanoparticles. *Anal Bioanal Chem*. 2016;408(18):5013–5019. doi:10.1007/s00216-016-9601-1
11. Zhang Y, Kohler N, Zhang M. Surface modification of superparamagnetic magnetite nanoparticles and their intracellular uptake. *Biomaterials*. 2002;23(7):1553–1561. doi:10.1016/S0142-9612(01)00267-8
12. Huff TB, Hansen MN, Zhao Y, Cheng JX, Wei A. Controlling the cellular uptake of gold nanorods. *Langmuir*. 2007;23(4):1596–1599. doi:10.1021/la062642r
13. Huang HC, Barua S, Kay DB, Rege K. Simultaneous enhancement of photothermal stability and gene delivery efficacy of gold nanorods using polyelectrolytes. *ACS Nano*. 2009;3(10):2941–2952. doi:10.1021/nn900784f
14. Pissuwan D, Niidome T. Polyelectrolyte-coated gold nanorods and their biomedical applications. *Nanoscale*. 2015;7(1):59–65. doi:10.1039/C4NR04350B
15. Nel A, Ruoslahti E, Meng H. New insights into "Permeability" as in the enhanced permeability and retention effect of cancer nanotherapeutics. *ACS Nano*. 2017;11(10):9567–9569. doi:10.1021/acsnano.7b07214
16. Shao H, Xu D, Ding Y, Hong X, Liu Y. An "off-on" colorimetric and fluorometric assay for Cu(II) based on the use of $NaYF_4$:Yb(III), Er(III) upconversion nanoparticles functionalized with branched polyethylenimine. *Mikrochim Acta*. 2018;185(4):211. doi:10.1007/s00604-018-2740-7
17. Sun S, Zeng H, Robinson DB, et al. Monodisperse MFe2O4 (M = Fe, Co, Mn) nanoparticles. *J Am Chem Soc*. 2004;126(1):273–279. doi:10.1021/ja047044i
18. Chen J, Chen S, Gao Y. Anisotropy enhancement of thermal energy transport in supported black phosphorene. *J Phys Chem Lett*. 2016;7(13):2518–2523. doi:10.1021/acs.jpclett.6b00858
19. Liu Z, Sneve M, Haroldson TA, Smith JP, Drewes LR. Regulation of monocarboxylic acid transporter 1 trafficking by the canonical Wnt/beta-catenin pathway in rat brain endothelial cells requires cross-talk with notch signaling. *J Biol Chem*. 2016;291(15):8059–8069. doi:10.1074/jbc.M115.710277
20. Watson AS, Soilleux EJ. Detection of p62 on paraffin sections by immunohistochemistry. *Cold Spring Harb Protoc*. 2015;2015(8):756–760. doi:10.1101/pdb.prot086280
21. Zolnik BS, Gonzalez-Fernandez A, Sadrieh N, Dobrovolskaia MA. Nanoparticles and the immune system. *Endocrinology*. 2010;151(2):458–465. doi:10.1210/en.2010-0412
22. Hu B, Mayer MP, Tomita M. Modeling Hsp 70-mediated protein folding. *Biophys J*. 2006;91(2):496–507. doi:10.1529/biophysj.106.088781